INSTITUTE OF PHYSICS PUBLISHING JOURNAL OF PHYSICS: CONDENSED MATTER

J. Phys.: Condens. Matter **13** (2001) 5295–5311 www.iop.org/Journals/cm PII: S0953-8984(01)20505-0

The structural and electronic properties of $(AlN)_x(C_2)_{1-x}$ and $(AlN)_x(BN)_{1-x}$ alloys

Jin-Cheng Zheng, Hui-Qiong Wang, C H A Huan and A T S Wee

Department of Physics, National University of Singapore, Lower Kent Ridge Road, Singapore 119260

Received 5 January 2001, in final form 20 February 2001

Abstract

The ground-state properties of (III–V)–(IV_2) type alloy $(AlN)_x(C_2)_{1-x}$ and (III–V)–(III–V) type alloy $Al_xB_{1-x}N$ have been studied by self-consistent calculations. The calculated results show that the solid solution between cubic AlN and C (diamond) and that between AlN and BN are both nonideal, and the nonideality of AlN–C_2 solid solution is larger than that of AlN–BN. The bulk modulus of $(AlN)_x(C_2)_{1-x}$ ($x = 0.25$, 0.5, 0.75) is less than that of $Al_xB_{1-x}N$ ($x = 0.25$, 0.5, 0.75), although the bulk modulus of diamond is larger than BN. The large positive formation energies of alloys $(AlN)_x(C_2)_{1-x}$ and $(AlN)_x(BN)_{1-x}$ indicate that these solid solutions are both metastable.

Band structures of bulk diamond, cubic BN and AlN show that they are all indirect wide band gap structures, where the conduction band minima are situated at the Δ k-point for diamond and the X k-point for BN and AlN. (III–V)–(IV_2) type AlN-diamond mixed crystals and alloys exhibit an anomalously large band gap bowing while (III^A–V)–(III^B–V) type AlN-BN systems show slightly bowing. The band line-ups of $(AlN)_x(C_2)_{1-x}/(AlN)_x(BN)_{1-x}$ show that these alloy heterojunctions will change from type-II heterojunction to type-I heterojunction.

1. Introduction

Recently, there has been increasing interest in to wide band gap semiconductors such as diamond, boron nitride, aluminum nitride and related wide band gap semiconductors [1–8]. There are several motivations for this interest. Firstly, wide band gaps are required for high-temperature applications and for electro-optical applications in the short-wavelength range of the visible spectrum and the near UV. Short wavelength semiconductor lasers are of interest to optical memory designers. By reducing the wavelength of the laser light used for reading and writing, greater bit densities can be realized. A semiconductor ultraviolet photodetector is of great interest to the petroleum and aviation industries which require *in situ* diagnostics at these wavelengths for oil drilling and aircraft engine combustion processes. These devices must not only be sensitive to the ultraviolet spectrum, but also be stable at high temperatures. The nitrides offer a wider bandgap range, better lattice matched alloys, and improved thermal

0953-8984/01/225295+17$30.00

stability when compared to the Zn based II–VI semiconductors, the other material system considered promising for these applications. Also, the notable doping problems [9] for II–VI compounds such as the selenides and tellurides of zinc and cadmium increases the interest of study for alternative materials, namely the nitrides [3, 10]. Secondly, diamond and cubic boron nitride (c-BN) have recently received considerable attention because of their extreme values of hardness, thermal conductivity, and elastic constants [2]. AlN has several outstanding physical properties that have attracted much interest. Its hardness, high thermal conductivity, resistance to high temperature and caustic chemicals makes AlN an attractive material for electronic packaging applications.

We chose two alloy systems to study and compare, i.e., (III–V)–(IV_2) type alloy $(AlN)_x(C_2)_{1-x}$ and (III–V)–(III–V) type alloy $Al_xB_{1-x}N$. Single-phase ternary $(A^{III}B^{V})_x(C_2^{IV})_{1-x}$ semiconductor alloys constitute a new class of metastable compounds with unusual structural, electronic and optical properties [3, 5–8, 11]. The heterojunctions between $(A^{III}B^{V})_x(C_2^{IV})_{1-x}$ semiconductor alloys showed anomalous behaviour of band alignment compared to that of isovalent (III–V)–(III–V) type, (II–VI)–(II–VI) and IV–IV alloys [8, 10–20].

More recently, there have been some reports on synthesis and characterization of AlN-BN alloys and AlN-C alloys. Cubic boron aluminum nitride alloys have been prepared by ion-beam assisted deposition [21]. The AlN+BN composites were produced by chemical vapour deposition (CVD) [22–24]. The diamond and AlN layered composites were analysed by Jagannadham [25], the composite coatings of AlN and diamond on silicon, copper and steel substrates were prepared and their tribological properties were investigated by Godbole and Narayan [26], and the aluminum carbonitride Al_5C_3N was observed in low-carbon dynamo steel containing 0.20–0.30% aluminum [27].

In this work, the self-consistent total energy calculations have been performed for (III–V)–(IV_2) type alloy $(AlN)_x(C_2)_{1-x}$ and (III–V)–(III–V) type alloy $Al_xB_{1-x}N$. The ground-state properties such as the equilibrium lattice constants, bulk moduli and their pressure derivative, formation energies and stability of these two alloys are presented. The electronic structures of these two alloys are presented. The differences between these two solid solutions (AlN–C_2 and AlN–BN) are compared and the ordered and disordered properties are also discussed. The band gap behaviours of the solid solutions and the band alignment of $(AlN)_x(C_2)_{1-x}/Al_xB_{1-x}N$ are also studied.

2. Methods of calculation

The total energies of five ordered structure alloys $(AlN)_n(C_2)_{4-n}$ and $(AlN)_n(BN)_{4-n}$ are calculated using the LMTO-ASA method with the Löwdin perturbation technique [13, 20]. Among the five ordered structures ($n = 0, 1, 2, 3, 4$), the $n = 0$ element (C) and compound (BN) and $n = 4$ compound (AlN) have diamond and zinc-blende (ZB) structures respectively. The $n = 2$ compound has a CuAu structure ($L1_0$), and $n = 1$ and 3 compounds have Luzonite ($L1_2$) structures [3, 6, 13, 14, 19]. In order to provide an adequate description of the charge density and potential in the interstitial regions, empty spheres (equal to the number of atoms in a unit cell) are added at suitable sites, while preserving the crystal symmetry [13, 15, 20]. The ratio of radii for B (or Al), N, and C atoms and empty spheres is 1:1:1:1. The special-*K*-point method [28] is adopted for the summation over the Brillouin zone.

The statistically averaged property of the disordered alloys is described by a cluster expansion, which is a generalization of the Connolly–Williams approach [29].

Firstly, we determine the equilibrium lattice constants of ordered $(AlN)_n(C_2)_{4-n}$ and $(AlN)_n(BN)_{4-n}$ by total energy calculations, and compare to the lattice constants of the ideal

mixing solid solution, i.e.,

$$a(n) = \frac{n}{4}a(\mathrm{AlN}) + \left(1 - \frac{n}{4}\right)a(\mathrm{C_2})$$

and

$$a(n) = \frac{n}{4}a(\mathrm{AlN}) + \left(1 - \frac{n}{4}\right)a(\mathrm{BN})$$

respectively. The nonideality of the molar volumes in the cubic AlN–BN and AlN–diamond solid solutions can be described with a standard mixing model where the excess volume term is given by $\Delta V^{KS} = x(1-x)(\delta W^G/\delta P)$ [5]. Here, x and $(1-x)$ are the mole fractions of cubic AlN, BN and C (diamond), and W^G is the interaction (or Margules) parameter.

The bulk modulus of ordered $(AlN)_n(C_2)_{4-n}$ and $(AlN)_n(BN)_{4-n}$ are calculated by fitting the total energy-volume to the Birch–Murnaghan equation of state [30],

$$E_{\mathrm{tot}}(V) = \frac{B_0 V}{B_0'}\left[\frac{(V_0/V)^{B_0'}}{B_0' - 1} + 1\right] + \mathrm{const} \tag{1}$$

where B_0 and B_0' are the bulk modulus and its pressure derivative at the equilibrium volume V_0. We also use Cohen's empirical formula [31, 32] to calculate the bulk modulus,

$$B_0 = \frac{N_c}{4}\frac{(1972 - 200I)}{d^{3.5}} \tag{2}$$

where N_c is the coordination number. An empirical ionicity parameter $I = 0$, 1, and 2 for group IV, III–V, and II–VI solids, respectively, accounts for the reduction in B_0 arising from increased charge transfer. For tetrahedral systems, $N_c = 4$; otherwise N_c is the average coordination number.

The energy of formation $E_{\mathrm{form}}(n)$ (normalized to eV per atom) for ordered structures is defined [6, 33] as, for $(AlN)_n(C_2)_{4-n}$ ordered structures

$$E_{\mathrm{form}}(n) = E_{(\mathrm{AlN})_n(C_2)_{4-n}} - \frac{n}{4}E_{\mathrm{AlN}} - \left(1 - \frac{n}{4}\right)E_{\mathrm{C_2}}. \tag{3a}$$

For $(AlN)_n(BN)_{4-n}$ ordered structures

$$E_{\mathrm{form}}(n) = E_{(\mathrm{AlN})_n(\mathrm{BN})_{4-n}} - \frac{n}{4}E_{\mathrm{AlN}} - \left(1 - \frac{n}{4}\right)E_{\mathrm{BN}}. \tag{3b}$$

The energy formation $E_{\mathrm{form}}(x)$ for disordered structures can be obtained from the results of ordered structures by a cluster expansion [6, 13, 29],

$$E_{\mathrm{form}}(x) = \sum_{n=0}^{4} P_n(x)E_{\mathrm{form}}^n \tag{4}$$

$$P_n(x) = \binom{4}{n}x^n(1-x)^{4-n} \tag{5}$$

where the $F_{\mathrm{form}}(x)$ is the energy of formation of disordered alloys, and E_{form}^n is the energy of formation of each of the above five ordered structures. $P_n(x)$ is the statistical weight, which is the probability that the nth short-range ordered structure occurs in the alloy.

3. Results and discussions

3.1. Lattice constant

The results of total energies E_{tot} (eV) as a function of lattice constants are obtained by the above method. The equilibrium lattice constants obtained from total energy calculations for

Table 1. Calculated lattice constants for C, BN and AlN compared with the experimental and other calculated results.

	a_0 (Å)
C	
Present calculation	**3.56**
Experiment	3.567 [5, 36, 37]
BN	
Present calculation	**3.61**
Experiment	3.617 [5], 3.616 [37]
AlN	
Present calculation	**4.38**
Experiment	4.37 [35][a]

[a] The lattice constant corresponds to the cubic structure with the equivalent volume per atom as the observed wurtzite structure.

C, cubic BN and AlN are compared with the experimental data in table 1. The lattice constants are in good agreement with the measured values.

The equilibrium lattice constants of ordered $(AlN)_x(C_2)_{1-x}$ and $(AlN)_x(BN)_{1-x}$ are calculated and listed in table 2 and plotted in figure 1(a). The calculated lattice constants of ordered structures $(AlN)_n(C_2)_{4-n}$ and $(AlN)_n(BN)_{4-n}$ ($n = 1, 2, 3$) are both larger than those of ideal mixing (Vegard's law) between the diamond and AlN, AlN and BN. The difference between calculated lattice constant and lattice constant of ideal mixing $\Delta a(x)$ is also listed in table 2 and plotted in figure 1(b). The differences $\Delta a(x)$ (excess lattice constant) of ordered $(AlN)_x(C_2)_{1-x}$ ($x = 0.25, 0.5, 0.75$) comparing to ideal mixing are about twice those of ordered $(AlN)_x(BN)_{1-x}$. The equilibrium unit-cell volumes are up to 11.8% and 5.4% larger than predicted values of ideal mixing (Vegard's law) for ordered structures $(AlN)_n(C_2)_{4-n}$ and $(AlN)_n(BN)_{4-n}$ respectively. These results indicate that the solid solutions of AlN–C_2 and AlN–BN are both nonideal, and the nonideality of ordered $(AlN)_x(C_2)_{1-x}$ is larger than that of ordered $(AlN)_x(BN)_{1-x}$.

Table 2. Equilibrium lattice constants $a_0(x)$ of ordered $(AlN)_x(C_2)_{1-x}$ and $(AlN)_x(BN)_{1-x}$ via x, and compared to that of ideal mixing crystals $a_i(x)$. The differences between total energy calculated results and those of ideal mixing are listed as $\Delta a(x)$.

	$(AlN)_x(C_2)_{1-x}$			$(AlN)_x(BN)_{1-x}$		
Composition (x)	$a_0(x)$	$a_i(x)$	$\Delta a(x)$	$a_0(x)$	$a_i(x)$	$\Delta a(x)$
0.00	3.56	3.56	0	3.61	3.61	0
0.25	3.88	3.77	0.11 (**2.8%**)	3.86	3.80	0.06 (**1.6%**)
0.50	4.12	3.97	0.15 (**3.6%**)	4.07	4.00	0.07 (**1.7%**)
0.75	4.28	4.18	0.10 (**2.4%**)	4.24	4.19	0.05 (**1.2%**)
1.00	4.38	4.38	0	4.38	4.38	0

3.2. Nonideality parameter

From the standard mixing model, the nonideality of AlN–C_2 and AlN–BN solid solutions are calculated and listed in table 3. The average nonideality parameter ($\delta W^G/\delta P$) of ordered $(AlN)_x(C_2)_{1-x}$ is 2.12 ± 0.14 J MPa^{-1}, while that of ordered $(AlN)_x(BN)_{1-x}$ is

Table 3. Nonideality parameter $(\delta W^G/\delta P)$ of ordered $(AlN)_x(C_2)_{1-x}$ and $(AlN)_x(BN)_{1-x}$.

Composition (x)	$(AlN)_x(C_2)_{1-x}$	$(AlN)_x(BN)_{1-x}$
0.25	1.98 J MPa^{-1}	0.99 J MPa^{-1}
0.50	2.17 J MPa^{-1}	1.07 J MPa^{-1}
0.75	2.21 J MPa^{-1}	1.10 J MPa^{-1}

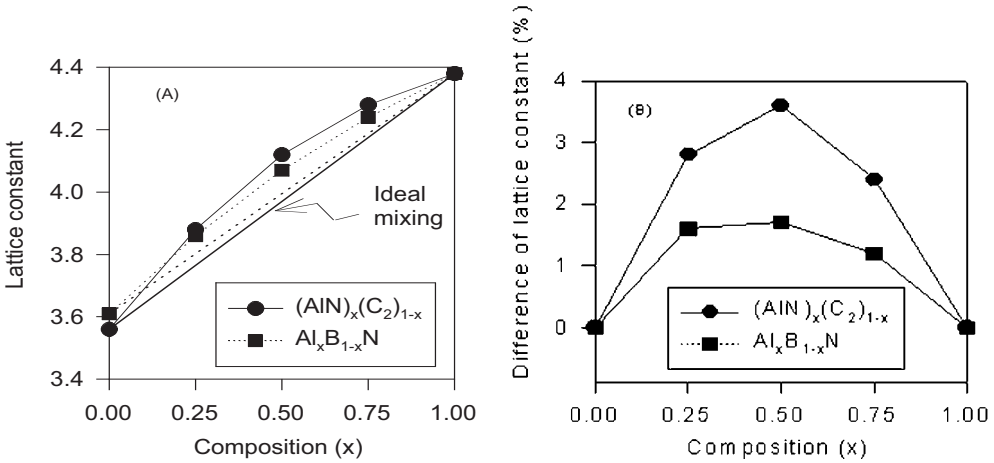

Figure 1. (a) The calculated lattice constants (circle symbol for AlN–C_2; square symbol for AlN–BN) and lattice constants of ideal mixing solid solutions (solid line for AlN–C_2; medium dashed line for AlN–BN) for five ordered structure alloys $(AlN)_n(C_2)_{4-n}$ and $(AlN)_n(BN)_{4-n}$ ($n = 0, 1, 2, 3, 4$). (b) The differences between calculated lattice constants and lattice constants of ideal mixing solid solutions, (symbols are calculated points; circle symbol for $(AlN)_n(C_2)_{4-n}$, square symbol for $(AlN)_n(BN)_{4-n}$). Lattice constant unit is in Å.

1.05 ± 0.06 J MPa^{-1}. They are both larger than the nonideality parameter of BN–C_2 solid solutions [6]. However, $\Delta a(x)$ and $(\delta W^G/\delta P)$ will be decreased due to (i) statistical averaging in disordered alloys, and (ii) the relaxation effect.

3.3. The equation of state

The equation of state for the solid state is often measured from pressure dependence x-ray diffraction (XRD) to determine elastic properties such as the bulk modulus [5]. We calculate the equation of state for these two ordered solid solutions AlN–C_2 and AlN–BN, and present the results in figure 2. The relationship of the strain volume V/V_0 (where V is volume under pressure, V_0 is the volume without pressure) under the same pressure ($p > 0$) among the different compositions of solid solutions AlN–C_2 and AlN–BN can be written as,

$$\begin{aligned}(V/V_0)_{\text{diamond}} &> (V/V_0)_{\text{BN}} > (V/V_0)_{(AlN)_1(BN)_3} > (V/V_0)_{(AlN)_1(C_2)_3} \\ &> (V/V_0)_{(AlN)_1(BN)_1} > (V/V_0)_{(AlN)_3(BN)_1} > (V/V_0)_{(AlN)_1(C_2)_1} \\ &> (V/V_0)_{(AlN)_3(C_2)_1} > (V/V_0)_{(AlN)}. \end{aligned} \tag{6}$$

The relationship shows that $(AlN)_n(C_2)_{4-n}$ can be compressed more easily than $(AlN)_n(BN)_{4-n}$ in the range $n = 1, 2, 3$, although BN can be compressed more easily than diamond. This anomalous behaviour will effect the bulk moduli of these two alloy systems.

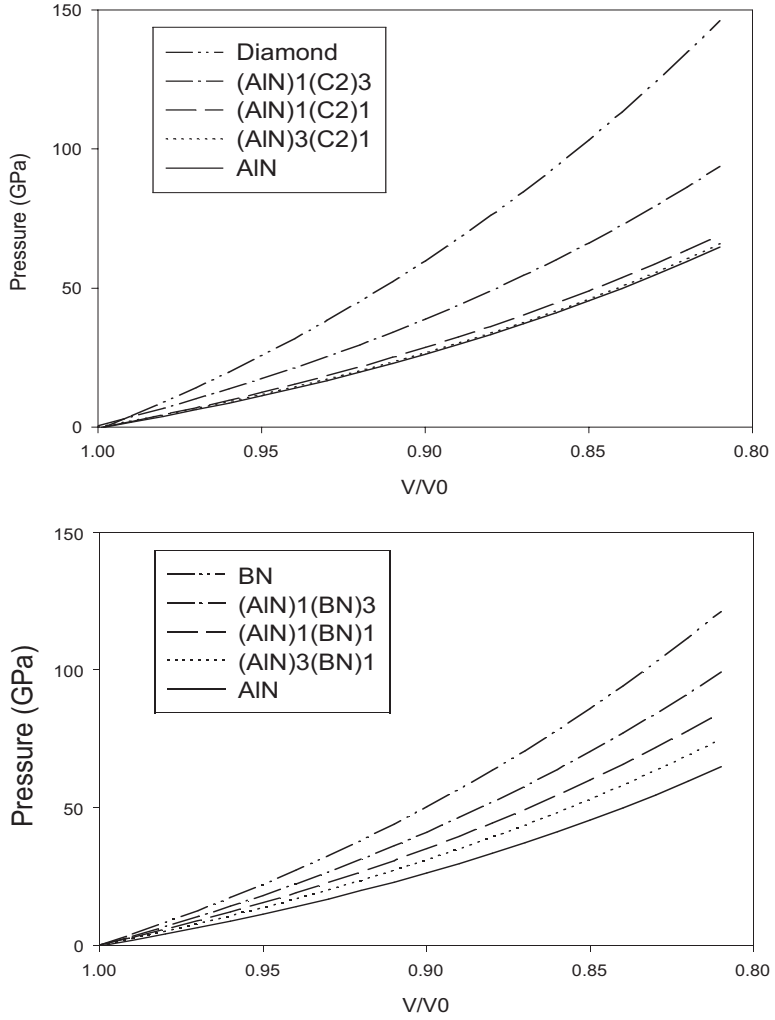

Figure 2. Calculated pressure–volume data for $(AlN)_n(C_2)_{4-n}$ and $(AlN)_n(BN)_{4-n}$ ($n = 0$, 1, 2, 3, 4). The curves for $(AlN)_n(C_2)_{4-n}$ from top to bottom are: the isothermal equations of state for diamond, $(AlN)_1(C_2)_3$, $(AlN)_1(C_2)_1$, $(AlN)_3(C_2)_1$ and AlN. (Also shown as the inset figure.) The curves for $(AlN)_n(BN)_{4-n}$ from top to bottom are: the isothermal equations of state for BN, $(AlN)_1(BN)_3$, $(AlN)_1(BN)_1$, $(AlN)_3(BN)_1$ and AlN. (Also shown as the inset figure.)

3.4. Bulk modulus

Hardness is one of the most important issues in the study of the ground-state properties of AlN–C_2 and AlN–BN solid solutions. Hardness involves the plastic deformation of materials which in turn depends critically on the motion of dislocations. Fully quantum-mechanical calculations of such properties are extremely difficult even with the state-of-the-art computational schemes and facilities [33]. The bulk modulus is often regarded as a measure of hardness of materials although it is not always positively correlated with the experimentally measured hardness.

We calculated the bulk modulus and its pressure derivatives of diamond, BN, and AlN both from equation (1) and equation (2). The results of diamond and BN compared to

experimental measurements and other theoretical results were presented in our previous study [6]. The present result of bulk modulus of AlN is 205 GPa from total energy calculations, 189 GPa from Cohen's empirical formula [31, 32] using our calculated value of bond length. The calculated result is in agreement with published experimental result of 206 GPa [34], and slightly smaller than another theoretical result of 215 GPa [35]. The agreement with experimental data demonstrated the validity of our calculations. The bulk moduli and their pressure derivatives from total energy results (equation (1)), bulk moduli from empirical formula (equation (2)), and the differences from ideal mixing for ordered $(AlN)_n(C_2)_{4-n}$ and $(AlN)_n(BN)_{4-n}$ are listed in table 4. The bulk moduli calculated using equation (1) are larger than those calculated using equation (2) for ordered $(AlN)_n(C_2)_{4-n}$ and $(AlN)_n(BN)_{4-n}$, except for the $L1_0$ structure $(AlN)_1(C_2)_1$. From figure 3, one can see that the bulk moduli of ordered $(AlN)_n(C_2)_{4-n}$ and $(AlN)_n(BN)_{4-n}$ are both smaller than those of ideal mixing, and the bulk moduli of ordered $(AlN)_n(C_2)_{4-n}$ are smaller than those of $(AlN)_n(BN)_{4-n}$ for the range $n = 1, 2, 3$, although the bulk modulus of diamond is larger than BN. The anomalous behaviour of $(AlN)_n(C_2)_{4-n}$ corresponds to its larger excess volume and high nonideality, compared to that of $(AlN)_n(BN)_{4-n}$, and it is also consistent with the behaviour of its equation of state.

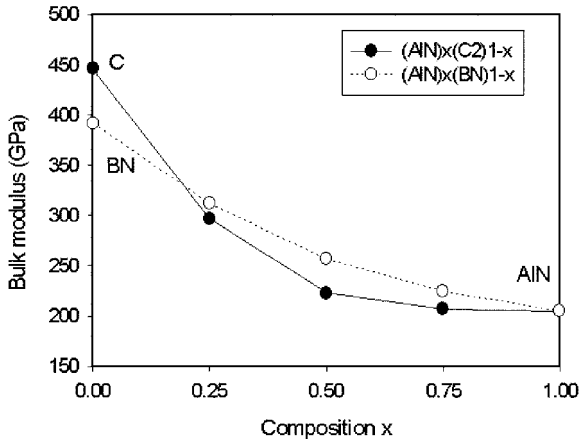

Figure 3. The total-energy calculated bulk moduli for ordered alloys $(AlN)_n(C_2)_{4-n}$ and $(AlN)_n(BN)_{4-n}$.

3.5. Formation energy

The energies of formation for $(AlN)_n(C_2)_{4-n}$ and $(AlN)_n(BN)_{4-n}$ ($n = 1, 2, 3$) were calculated and listed in table 5 and plotted in figure 4 together with those for disordered structures. The positive energy of formation for the entire concentration range at $T = 0$ indicates that it is energetically unfavourable for AlN and diamond, AlN and BN to mix and form alloys. The energies of formation of disordered alloys are lower than those of ordered alloys. The statistical averaging simply leads to renormalization by a factor of about 3/4. The positive energy of formation for $(AlN)_n(C_2)_{4-n}$ is larger than that for $(AlN)_n(BN)_{4-n}$ in the range $n = 1, 2, 3$. This can be explained by undersaturated (e.g., Al–C) and oversaturated (e.g. C–N) bonds in $(AlN)_n(C_2)_{4-n}$. The undersaturated and oversaturated bonds will lead to the charge compensation and charged *donor* and *acceptor* bonds which cost electrostatic energy. This causes the higher formation energy of $(AlN)_n(C_2)_{4-n}$ than $(AlN)_n(BN)_{4-n}$. The

Table 4. Calculated bulk moduli, their pressure derivatives from total energy results (equation (1)), bulk moduli from empirical formula (equation (3)), and the differences from ideal mixing.

	Equation (1)				Equation (3)			
			Differences from ideal mixing				Differences from ideal mixing	
	B_0	B_0'	$B_0 - B_i$	$(B_0 - B_I)/B_i(\%)$	d	B_0	$B_0 - B_i$	$(B_0 - B_i)/B_i(\%)$
C	446	3.45			1.54	433		
$(AlN)_1(C_2)_3$	297	3.84	−89	−23.1	1.68	289	−83	−22.3
$(AlN)_1(C_2)_1$	223	3.99	−103	−31.5	1.78	234	−107	−31.4
$(AlN)_3(C_2)_1$	207	3.87	−58	−21.9	1.85	204	−46	−18.4
AlN	205	3.91			1.90	189		
BN	392	3.79			1.56	371		
$(AlN)_1(BN)_3$	312	3.87	−33	−9.5	1.67	294	−32	−9.8
$(AlN)_1(BN)_1$	257	3.77	−42	−13.9	1.76	244	−36	−12.9
$(AlN)_3(BN)_1$	225	3.93	−27	−10.7	1.84	211	−24	−10.2
AlN	205	3.91			1.90	189		

band gap of $(AlN)_x(C_2)_{1-x}$ and band lineup of $(AlN)_x(C_2)_{1-x}/(AlN)_x(BN)_{1-x}$ heterojunction will be affected by the undersaturated and oversaturated bonds too. The band gap of $(AlN)_x(C_2)_{1-x}$ shows anomalously strong bowing comparing to that of $(AlN)_x(BN)_{1-x}$ and the alignment of $(AlN)_x(C_2)_{1-x}/(AlN)_x(BN)_{1-x}$ heterojunction will transfer from type-II to type-I heterojunction with increasing of composition x, as we will discuss in the following sections.

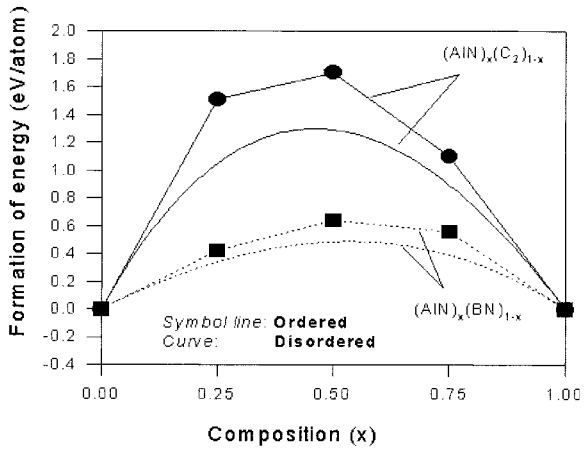

Figure 4. The calculated energy of formation for ordered structure (circle symbol for $(AlN)_n(C_2)_{4-n}$; square symbol for $(AlN)_n(BN)_{4-n}$) and disordered alloys (solid line for $(AlN)_x(C_2)_{1-x}$; dotted line for $(AlN)_x(BN)_{1-x}$). The energies of formation of disordered alloys are lower than that of ordered structure, both for AlN–C_2 and AlN–BN solid solutions.

3.6. Bulk band structure of diamond, BN and AlN

The bulk band structures of diamond, BN and AlN are shown in figure 5(a). The minimum of the conduction band occurs at point X for BN and AlN, and close to point X along the Δ

Table 5. The calculated energy of formation for ordered structure and disordered alloys.

		E_{form} (eV/atom)			E_{form} (eV/atom)	
n	$(AlN)_n(C_2)_{4-n}$	Ordered	Disordered	$(AlN)_n(BN)_{4-n}$	Ordered	Disordered
1	$(AlN)_1(C_2)_3$	1.51	1.05	$(AlN)_1(BN)_3$	0.42	0.34
2	$(AlN)_1(C_2)_1$	1.70	1.29	$(AlN)_1(BN)_1$	0.64	0.49
3	$(AlN)_3(C_2)_1$	1.10	0.89	$(AlN)_3(BN)_1$	0.56	0.39

axis in diamond. In figure 5(b), we also present the band structures of pure diamond, BN, and AlN in the thin 1+1 superlattice Brillouin zone, which will be easy to compare with the band structure of 1+1 superlattice $AlBN_2$ and $AlNC_2$ along [001] in the next section.

3.7. Band structure of $AlNC_2$ and $AlBN_2$

The band structures of the thin 1+1 superlattice AlN–C_2 and AlN–BN are shown in figure 6. The 1+1 superlattice is a (1+1) (001) superlattice and simultaneously a (110) superlattice. The Brillouin zone of the 1+1 superlattice is tetragonal. As explained by Lambrecht *et al* [48], the bands in tetragonal Brillouin zone are folded along those directions of the fcc Brillouin zone. For example, the bands along the tetragonal Γ–Z and Γ–X lines are the folded bands along the fcc Γ–X and Γ–K–X lines, respectively. This leads to numerous degeneracies at the ends of the Γ–Z and Γ–X axes of the tetragonal zone. The presence of such splitting is due to the fact that in representing the cubic band structure in the tetragonal Brillouin zone, certain symmetries associated with the diamond, BN and AlN structures are ignored. As can be seen from a comparison of the figures, these degeneracies are lifted in the bands of the tetragonal $AlNC_2$ and $AlBN_2$, which are similar to the BNC_2 case [48]. The magnitude of the splittings is an indication of the strength of the (noncubic) perturbation of the original band structure due to the superlattice formation [48]. Strong perturbations can be seen in bands, which are consistent with the large energy of formation of these superlattices.

One may notice that [48], due to the folding of the conduction-band minimum of BN and AlN at the X point of the fcc zone to the Γ point of the tetragonal zone, the band gaps of $AlNC_2$ and $AlBN_2$ effectively become direct. Although the matrix elements coupling this state to the valence-band maximum might still be weak, the optical transition between these states is no longer strictly forbidden by symmetry. The band gap of the 1+1 superlattice is considerably reduced compared to the bulk solids. Especially, for $AlNC_2$, the band structure shows zero band gap in the Γ point under LDA. Considering the GW correction, the band gap will be open to an amount of eV, but will be still quite small, compared with bulk diamond and AlN. We will discuss the band gap behaviours of $(AlN)_x(C_2)_{1-x}$and $(AlN)_x(BN)_{1-x}$ in detail in the following sections.

3.8. Band gap of $(AlN)_n(C_2)_{4-n}$ and $(AlN)_n(BN)_{4-n}$

We start with a discussion of the band gaps of the pure materials. As is well known, the band gaps are underestimated in the local-density-functional theory [3, 35, 42–44, 47, 48]. There is no exact justification for identifying the Kohn–Sham eigenvalues with quasiparticle excitations except for the highest occupied eigenvalue [38, 39]. The discrepancy between band gap and experimental data could either be due to the LDA itself, or due to the existence of a discontinuity in the exchange–correlation potential [40, 41], or to a combination of both. In spite of this controversy, it is well accepted that Hedin's GW approach can provide accurate quasiparticle

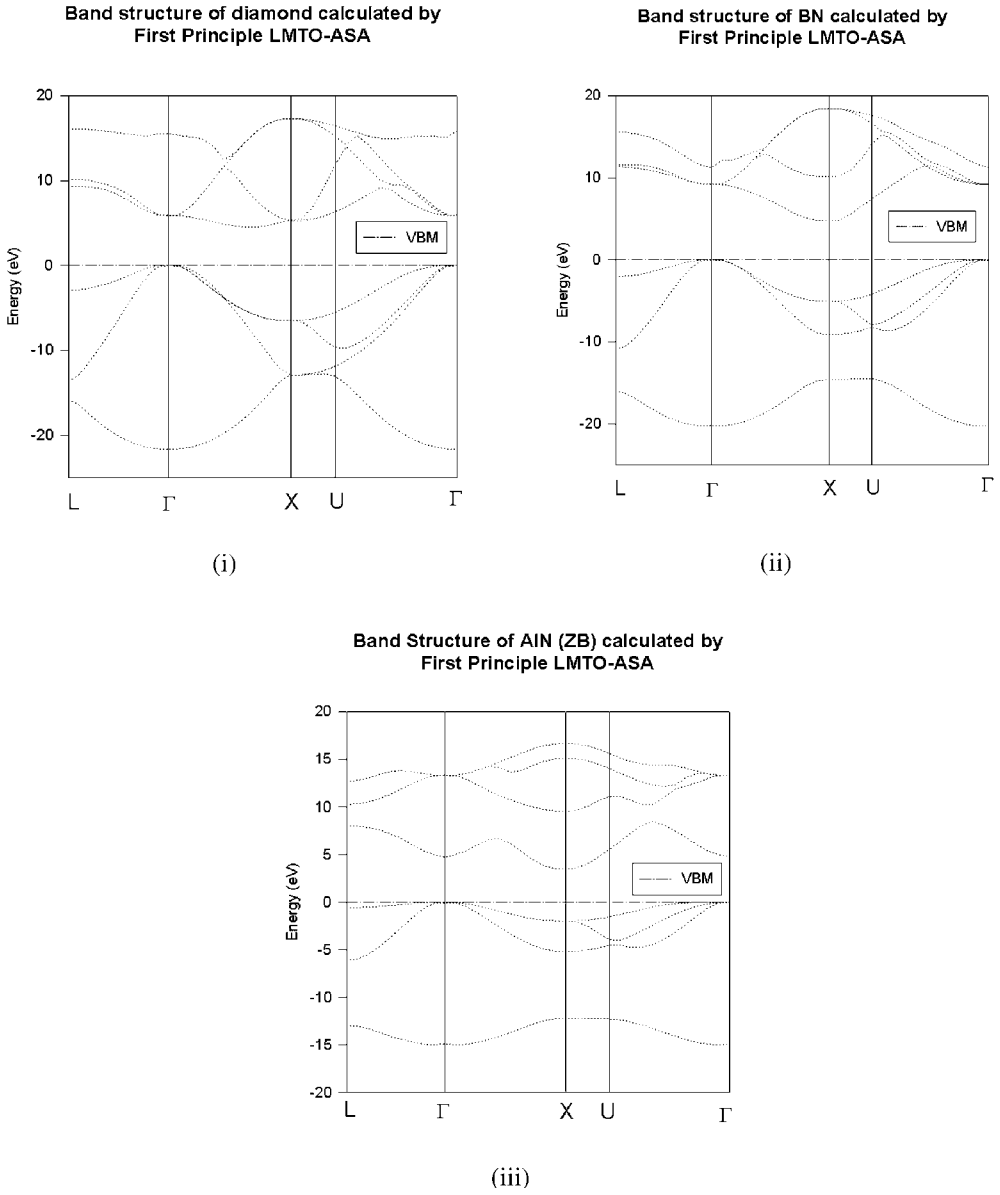

Figure 5. (a) Band structure of diamond (i), BN (ii), and AlN (iii) along symmetry lines of the fcc Brillouin zone by LMTO-ASA. (b) Band structure of diamond (i), BN (ii), and AlN (iii) along symmetry lines of the tetragonal Brillouin zone by LMTO-ASA.

energies [42–44]. Unfortunately, this approach requires very complex computations. On the other hand, Bechstedt and Del Sole [45] have made a simplified tight-binding analysis of the GW approach and obtained a simple analytic expression for the correction to the LDA band gap,

$$\Delta = \frac{e^2}{\varepsilon_\infty} q_{TF} \Big/ \left[1 + 7.62 q_{TF} \left(\frac{(1-\alpha_P) r_A}{2} + \frac{(1+\alpha_P) r_B}{2} \right) \right]. \tag{7}$$

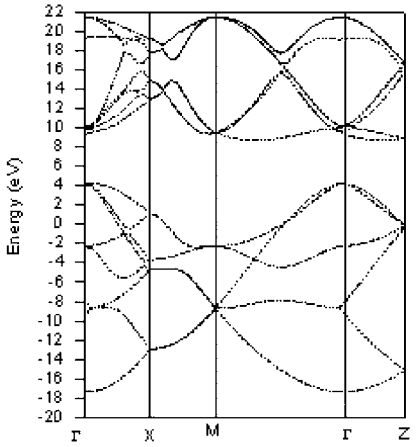

Band structure of C
along symmetry lines of
the tetragonal Brillouin zone.

(i)

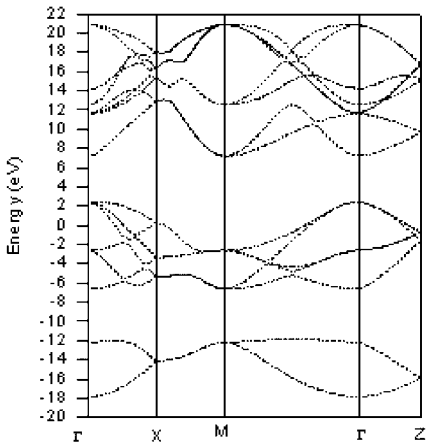

Band structure of BN
along symmetry lines of
the tetragonal Brillouin zone.

(ii)

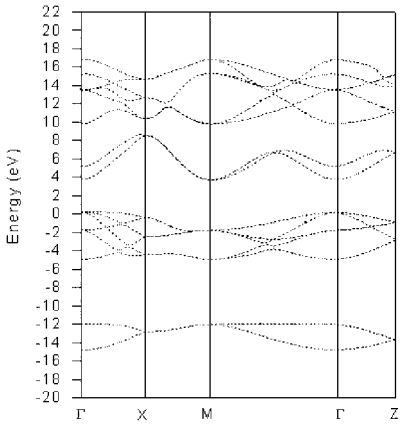

Band structure of AlN
along symmetry lines of
the tetragonal Brillouin zone.

(iii)

Figure 5. (*Continued.*)

In equation (7), q_{TF} is the Thomas–Fermi wave number, α_P is the polarizability (as defined by Harrison [46]), $r_{A(B)}$ are the cation and anion ionic radii, and ε_∞ is the high-frequency (electronic) dielectric constant. The simplest approach to including the effect of the self-energy correction is to shift the conduction bands up by a constant, the so-called scissors operation [35]. In the case of C and BN, these shifts are about 1.5 and 1.9 eV respectively [48]. However, under the internal summation approach used in this work the resulting LDA

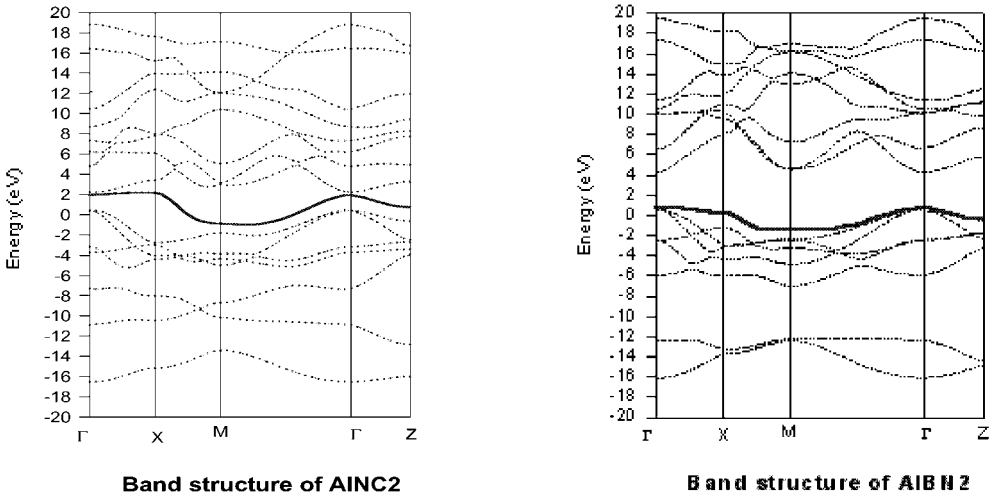

Figure 6. Band structure of $(AlN)_1(C_2)_1$ and $(AlN)_1(BN)_1$ along symmetry lines of the tetragonal Brillouin zone by LMTO-ASA.

band gaps are somewhat larger than those given by the normal LMTO–ASA method. With a shift of 1.08 eV (for C) and 1.42 eV (for BN) the theoretical and experimental bulk limit of the band gap is recovered. For cubic AlN, there is not experimental value available. We use the GW band gap of AlN (4.9 eV) [47] as reference, then the shift is 1.43 eV. The corrected band gaps of the alloys are obtained by the linear correction of related terminated bulk materials. The results with and without correction are listed in table 6. For the disordered phase, the band gap can be obtained from that of the ordered phase using the atomic cluster expansion:

$$E_g(x) = \sum_{n=0}^{4} P_n(x) E_g^n. \tag{8}$$

The following results can be obtained.
For $(AlN)_n(C_2)_{4-n}$ under LDA:

$$E_g(x) = 4.42 - 11.84x + 10.02x^2 + 1.6x^3 - 0.73x^4. \tag{9}$$

For $(AlN)_n(BN)_{4-n}$ under LDA:

$$E_g(x) = 4.68 - 2.96x + 1.62x^2 + 0.4x^3 - 0.27x^4. \tag{10}$$

For $(AlN)_n(C_2)_{4-n}$ with correction:

$$E_g(x) = 5.5 - 11.48x + 10.02x^2 + 1.56x^3 - 0.7x^4. \tag{11}$$

For $(AlN)_n(BN)_{4-n}$ with correction:

$$E_g(x) = 6.1 - 2.96x + 1.62x^2 + 0.4x^3 - 0.26x^4. \tag{12}$$

3.9. Band line-up of $(AlN)_x(C_2)_{1-x}$/$(AlN)_x(BN)_{1-x}$ alloy heterojunctions

3.9.1. Band offset of C/BN heterojunction The valence-band offsets (VBOs) at semiconductor heterointerfaces are the most important parameters in determining the electrical

Table 6. Band gap of $(AlN)_n(C_2)_{4-n}$ and $(AlN)_n(BN)_{4-n}$ (*ordered and disordered*).

		E_g (eV)		E_g (eV)	
n	$(AlN)_n(C_2)_{4-n}$	Ordered (LDA)	Ordered (correction)	Disordered (LDA)	Disordered (correction)
0	C_2	4.42	5.5	4.42	5.5
1	$(AlN)_1(C_2)_3$	1.46	2.63	2.11	3.28
2	$(AlN)_1(C_2)_1$	0.17	1.43	1.16	2.42
3	$(AlN)_3(C_2)_1$	0.95	2.29	1.62	2.96
4	AlN	3.47	4.9	3.47	4.9
		E_g (eV)		E_g (eV)	
n	$(AlN)_n(BN)_{4-n}$	Ordered (LDA)	Ordered (correction)	Disordered (LDA)	Disordered (correction)
0	BN	4.68	6.1	4.68	6.1
1	$(AlN)_1(BN)_3$	3.94	5.36	4.05	5.47
2	$(AlN)_1(BN)_1$	3.47	4.89	3.64	5.06
3	$(AlN)_3(BN)_1$	3.37	4.79	3.45	4.87
4	AlN	3.47	4.9	3.47	4.9

and optical properties of heterojunctions and superlattices. Because of its importance, this topic has stimulated a great deal of experimental and theoretical research work recently. The valence-band offset consists of two contributions, the first of which we may call the initial band offset, i.e., the difference between the positions of the valence-band maxima in each bulk crystal with respect to the ASA reference level [48]. It was found to be 1.79 eV, with diamond having the higher valence-band maximum in C/BN heterojunction. The other contribution is the interface dipole potential [48]. Only the total band offset has a physical significance, which can be determined by average-bond-energy theory [20], as we show later.

Based on average-bond-energy theory [20], the total valence-band offset of C/BN can be determined by,

$$\Delta E_v = E_{vm}^{C2} - E_{vm}^{BN} \tag{13}$$

where E_{vm}^{C2} and E_{vm}^{BN} are valence-band-offset parameters [13, 14, 19] which can be obtained by,

$$E_{vm} = E_v - E_m \tag{14}$$

where E_v is the valence-band maximum and E_m is average bond energy, which can be got from average-bond-energy theory [12–20], see the following equations

$$E_m = (E_b + E_a)/2 \tag{15}$$

$$E_b = \frac{1}{MN}\sum_{n=1}^{M}\sum_{k} En(k) \tag{16}$$

$$E_a = \frac{1}{MN}\sum_{n=m+1}^{2M}\sum_{k} En(k) \tag{17}$$

where N is the number of unit cells and M the number of valence bands. For the ZB, $L1_0$ and $L1_2$ structures, M is set equal to 4, 8 and 16, respectively.

Table 7. E_v, E_m, E_{vm} and E_{cm} for diamond and BN under LDA.

	E_v (eV)	E_m (eV)	E_{vm} (eV)
Diamond	4.2325	5.3682	−1.1357
BN	2.4349	4.9187	−2.4838

Using the parameters listed in table 7, one can calculate the valence-band offset of heterojunction C/BN by equation (13) as,

$$\Delta E_v(\mathrm{C/BN}) = 1.35\ \mathrm{eV} \tag{18}$$

which is consistent with previous results, 1.4 ± 0.05 eV [48] and 1.42 ± 0.04 eV [49]. While because

$$\Delta E_g(\mathrm{C/BN}) = -0.6\ \mathrm{eV} \tag{19}$$

the conduction-band offset can be also determined as,

$$\Delta E_c(\mathrm{C/BN}) = \Delta E_v(\mathrm{C/BN}) + \Delta E_g(\mathrm{C/BN}) = 0.75\ \mathrm{eV}. \tag{20}$$

3.9.2. Band offset of $(AlN)_x(C_2)_{1-x}/(AlN)_x(BN)_{1-x}$ alloy heterojunction The valence-band offset parameter $E_{vm}(x)$ and conduction-band offset parameter $E_cm(x)$ of the alloy $(\mathrm{AlN})_x(\mathrm{C_2})_{1-x}$ and $(\mathrm{AlN})_x(\mathrm{BN})_{1-x}$ can be obtained by the cluster expansion method, in terms of the data of the five ordered structures listed in table 8, i.e.,

$$E_{vm}(x) = \sum_n P_n(x) E^n_{vm} \tag{21a}$$

$$E_{cm}(x) = \sum_n P_n(x) E^n_{cm} \tag{21b}$$

where the statistical weight $P_n(x)$ is the possibility that the n short region ordered structure occurs in the alloy, and can be obtained from equation (5). $E_{cm}(x)$ and E^n_{cm} are the conduction-band offset parameters for disordered and ordered alloy respectively. With equation (21), we can get the valence-band-offset parameter for $(\mathrm{AlN})_x(\mathrm{C_2})_{1-x}$ as,

$$E_{vm}(x) = -1.151 + 2.8572x - 3.3402x^2 - 4.2640x^3 + 2.7853x^4 \tag{22}$$

and that for $(\mathrm{AlN})_x(\mathrm{BN})_{1-x}$ is,

$$E_{vm}(x) = -2.4772 + 0.0244x - 0.5286x^2 - 0.4688x^3 + 0.3375x^4. \tag{23}$$

So that the valence-band offset of alloy heterojunction $(\mathrm{AlN})_x(\mathrm{C_2})_{1-x}/(\mathrm{AlN})_x(\mathrm{BN})_{1-x}$ can be obtained as,

$$\Delta E_v(x) = 1.3262 + 2.8328x - 2.8116x^2 - 3.7952x^3 + 2.4478x^4. \tag{24}$$

Figure 8 plots $E_{vm}(x)$ and $E_{cm}(x)$ for $(\mathrm{AlN})_x(\mathrm{C_2})_{1-x}$ and $(\mathrm{AlN})_x(\mathrm{BN})_{1-x}$. From this figure, one can calculate the valence-band offset (VBO) and conduction-band offset (CBO) using average-bond-energy theory (i.e., for VBO, using equation (21*a*), for CBO, the formula is similar with equation (21*b*). It is also clearly shown that the heterojunction $(\mathrm{AlN})_x(\mathrm{C_2})_{1-x}/(\mathrm{AlN})_x(\mathrm{BN})_{1-y}$ can be a type-II ($x < 0.15$) or type-I ($x > 0.15$) heterojunction.

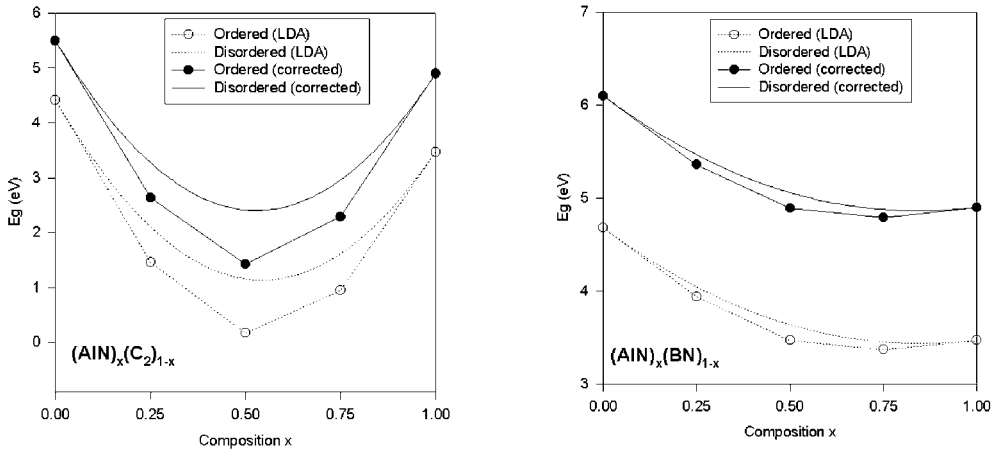

Figure 7. Band gap of ordered and disordered alloys for AlN–C_2 and AlN–BN solid solutions. The results of LDA (ordered and disordered) and corrections (ordered and disordered) are indicated in the figure.

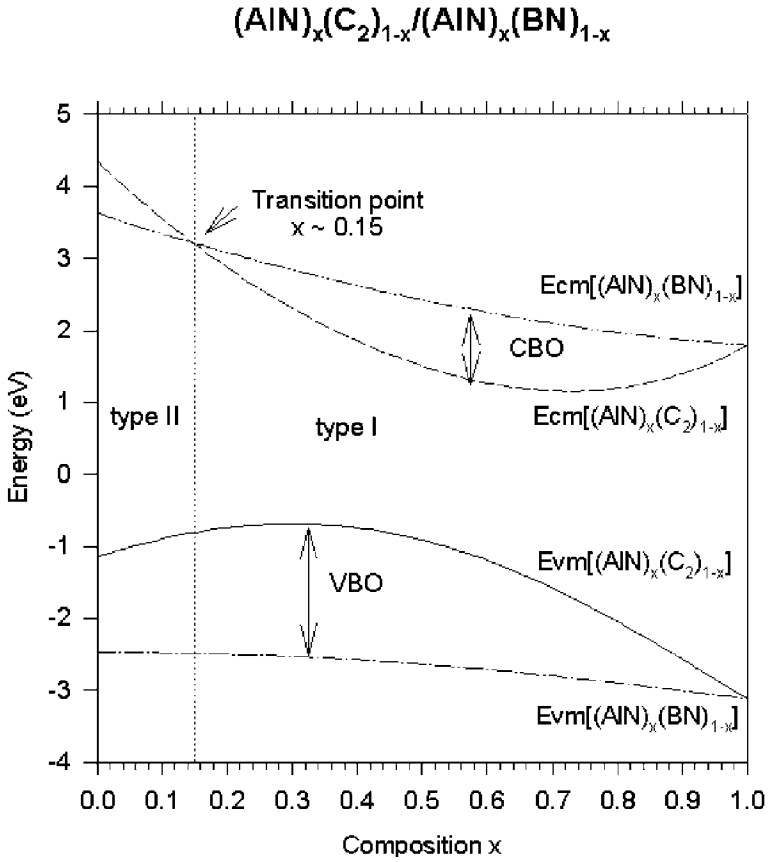

Figure 8. $E_{vm}(x)$ and $E_{cm}(x)$ for $(AlN)_x(C_2)_{1-x}$ and $(AlN)_x(BN)_{1-x}$.

Table 8. E_v, E_m, and E_{vm} for $(AlN)_x(C_2)_{1-x}$ and $(AlN)_x(BN)_{1-x}$ under LDA.

$(AlN)_x(C_2)_{1-x}$	E_v (eV)	E_m (eV)	E_{vm} (eV)
$x = 0.25$	2.6377	3.0744	−0.4367
$x = 0.5$	1.9540	2.2331	−0.2791
$x = 0.75$	0.8566	2.6008	−1.7442
$(AlN)_x(BN)_{1-x})$	E_v (eV)	E_m (eV)	E_{vm} (eV)
$x = 0.25$	1.2921	3.7632	−2.4711
$x = 0.5$	0.7110	3.2641	−2.5531
$x = 0.75$	0.3301	3.1705	−2.8404

4. Conclusion

In this work, the study of ground-state properties and electronic properties of cubic C–AlN and BN–AlN solid solutions from first-principle calculations are presented. The total energy, equilibrium lattice constant, bulk modulus and its pressure derivative and cohesive energy of mixed crystals of diamond and cubic (ZB) AlN, cubic (ZB) BN and AlN have been calculated by the first principle LMTO-ASA method with the Lowdin perturbation technique.

The calculated results show that the solid solution between cubic AlN and C (diamond) is nonideal. The nonideality of AlN–C_2 solid solution is larger than that of AlN–BN. The bulk modulus of $(AlN)_n(C_2)_{4-n}$ ($n = 1, 2, 3$) is less than that of $(AlN)_n(BN)_{4-n}$ ($n = 1, 2, 3$), although the bulk modulus of diamond is large than BN. The large positive formation energy of alloys $(AlN)_x(C_2)_{1-x}$ and $(AlN)_x(BN)_{1-x}$ indicate that these solid solutions are both metastable. The nonideality and formation energy of solid solutions decrease for disordered alloys compared to ordered structures.

The electronic properties of bulk diamond, cubic (ZB) BN and AlN and their mixed crystals have also been investigated in this paper. The band structures of bulk diamond, cubic BN and AlN show that they are all indirect wide band gap structures, where the conduction band minima are situated at the Δ k-point for diamond and the X k-point for BN and AlN. (III–V)–(IV_2) type AlN–diamond mixed crystals and alloys exhibit an anomalously large band gap bowing while (III^A–V)–(III^B–V) type AlN–BN systems show slight bowing. The band line-ups of $(AlN)_x(C_2)_{1-x}/(AlN)_x(BN)_{1-x}$ show that these alloy heterojuctions will change from type-II heterojuctions to type-I heterojunctions.

Acknowledgment

The authors thank Professor Ren-Zhi Wang in The Department of Physics, Xiamen University (China) for his help on the computational methods.

References

[1] Glass J T, Messier R and Fujimori N (eds) 1990 Diamond, Boron Nitride, Silicon Carbide and Related Wide bandgap Semiconductors *MRS Symposia Proc. No 162* (Pittsburgh: Materials Research Society)

[2] Pouch J J and Alterovitz S A (eds) 1990 Synthesis and properties of Boron Nitride *Materials Science Forum*, Vol 54 and 55 (Aldermannsdorf: Trans Tech)

Pouch J J and Alterovitz S A (eds) 1989 Properties and characterization of amorphous carbon *Materials Science Forum*, Vol 54 and 55 (Aldermannsdorf: Trans Tech)

[3] Lambrecht W R L and Segall B 1993 *Phys. Rev.* B **47** 9289

[4] Morkoc H, Strite S, Gao G B, Lin M E, Sverdlov B and Burns M 1994 *J. Appl. Phys.* **76** 1363

[5] Knittle E, Kaner R B, Jeanloz R and Cohen M L 1995 *Phys. Rev.* B **51** 12149 and references therein
[6] Zheng J C, Huan C H A, Wee A T S, Wang R Z and Zheng Y M 1999 *J. Phys.: Condens. Matter* **11** 927
[7] Zheng J C, Huan C H A and Wee A T S *APSIA Conference '98, Singapore (Asia-Pacific Surface & Interface Analysis Conference, 1998)* No Me-P-1
[8] Zheng J C, Huan C H A, Wee A T S and Guo Y P *APSIA Conference '98, Singapore (Asia-Pacific Surface & Interface Analysis Conference, 1998)* No Me-3-2
[9] Schetzina J F, Bartoli F J Jr. and Schaake H F (eds) 1990 Properties of II–VI semiconductors: Bulk Crystals, Epitaxial Films, Quantum Well Structures, and Dilute Magnetic Systems, *MRS Symposia Proc. No 161* (Pittsburgh: Materials Research Society)
[10] Cai S H, Wang R Z, Zheng Y M and Zheng J C 1998 *Chinese J. Lumin.* **18** 293
[11] Osorio R, Froyen S and Zunger A 1991 *Phys. Rev.* B **43** 14055 and references therein
[12] Zheng Y M, Wang R Z, Zheng J C and He G M 1996 *J. Xiamen University, (Natural Sci.)* **35** 705 (in Chinese)
[13] Zheng J C, Zheng Y M and Wang R Z 1997 *J. Phys.: Conden. Matter*. **9** 439
[14] Zheng J C, Zheng Y M and Wang R Z 1997 *Chinese Phys. Lett.* **14** 775
[15] Cai S H, Zheng J C, Wang R Z and Zheng Y M 1997 *Chinese J. Comput. Phys.* **14** 542
[16] Zheng J C, Wang R Z and Zheng Y M 1998 *Res. Prog. Solid State Electron.* **18** 20
[17] Wang H Q, Zheng J C, Wang R Z, Zheng Y M and Cai S H *APSIA Conference '98, Singapore (Asia-Pacific Surface & Interface Analysis Conference, 1998)* No Mi-P-8
[18] Wang H Q, Zheng J C, Wang R Z, Zheng Y M, Cai S H and Li S P *APSIA Conference '98, Singapore (Asia-Pacific Surface & Interface Analysis Conference, 1998)* No Mi-P9
[19] Wang H Q, Zheng J C, Wang R Z, Zheng Y M and Cai S H 1999 *Surf. Interface Anal.* **28** 177
[20] Wang R Z, Ke S H and Huang M C 1992 *J. Phys.: Condens. Matter* **4** 8083
[21] Edgar J H, Smith D T, Eddy C R, Carosella C A and Sartwell B D 1997 *Thin Solid Films* **298** 33
[22] Hanigofsky J A, More K L, Lackey W J, Lee W Y and Freeman G B 1991 *J. Am. Ceram. Soc.* **74** 301
[23] Lee W Y, Lackey W J, Agrawal P K and Freeman G B 1991 *J. Am. Ceram. Soc.* **74** 2649
[24] Dou D, Ketchum D R, Hamilton E J M, Florian P A, Vermillion K E, Grandinetti P J and Shore S G 1996 *Chem. Mat.* **8** 2839
[25] Jagannadham K 1999 *J. Vac. Sci. Tech.* A **17** 373
[26] Godbole V P and Narayan J 1996 *Mat. Sci. Eng.* B **39** 153
[27] Slavov V I, Naumova O M, Spevak E Y, Zadornaya V N and Tishkov V Y 1995 *Russ. Metall.* **1** 65
[28] Chadi D J and Cohen M L 1973 *Phys. Rev.* B **8** 5747
[29] Connolly J W D and Williams A R 1983 *Phys. Rev* B **27** 5169
[30] Murnaghan F D 1944 *Proc. Natl Acad. Sci.* **30** 244
[31] Cohen M L 1985 *Phys. Rev.* B **32** 7988
[32] Cohen M L 1993 *Science* **261** 307
[33] Jhi S H and Ihm J 1997 *Phys. Rev.* B **56** 13826
[34] Boch P, Glandus J C, Jarrige J and Lecompte J P 1982 *Ceram. Int.* **8** 34
[35] Lambrecht W R L and Segall B 1991 *Phys. Rev.* B **43** 7070
[36] Yin M T 1984 *Phys. Rev.* B **30** 1773
[37] Madelung O (ed) 1982 *Landolt–Bornstein tables (Landolt–Bornstein: Numerical Data and Functional Relationships in Science and Technology, New Series)* vol 17a (Berlin: Springer)
[38] Almbladh C O and von Barth U 1985 *Phys. Rev.* B **31** 3231
[39] Sham L J and Kohn W 1966 *Phys. Rev.* **145** 561
[40] Perdew L P and Levy M 1983 *Phys. Rev. Lett.* **51** 1884
[41] Sham L J and Schlüter M 1983 *Phys. Rev. Lett.* **51** 1888
[42] Godby R W, Schlüter M and Sham L J 1986 *Phys. Rev. Lett.* **56** 2415
Godby R W, Schlüter M and Sham L J 1988 *Phys. Rev.* B **37** 10159
[43] Hybertsen M S and Louie S G 1985 *Phys. Rev. Lett.* **55** 1418
Hybertsen M S and Louie S G 1986 *Phys. Rev.* B **34** 5390
[44] Hanke W and Sham L J 1988 *Phys. Rev.* B **38** 13361
[45] Bechstedt F and Del Sole 1988 *Phys. Rev.* B **38** 7710
[46] Harrison W A 1990 *Electronic Structure and Properties of Solids* (San Francisco: Freeman)
[47] Rubio A, Corkill J L, Cohen M L, Shirley E L and Louie S G 1993 *Phys. Rev.* B **48** 11810
[48] Lambrecht W R L and Segall B 1989 *Phys. Rev.* B **40** 9909
[49] Pickett W E 1988 *Phys. Rev.* B **38** 1316